# SHOULDER END MILLS WITH PCD INSERTS SHARPENED BY DIFFERENT ELECTRICAL TECHNOLOGIES

**TOMAS TRCKA, ALES POLZER, JOSEF SEDLAK**

Brno University of Technology,
Faculty of Mechanical Engineering, Brno, Czech Republic

**DOI: 10.17973/MMSJ.2018_11_201822**

**e-mail:** 153306@vutbr.cz

Diamond materials are increasingly used in machining processes as a cutting material, due to their specific properties. Nowadays, is a natural diamond successively replaced by an man-made - synthetic diamond, what also increases their availability. The most used diamond material for milling operations is a synthetic polycrystalline diamond (PCD) produced by HPHT (high-pressure high-temperature) process, because the high fracture toughness of the tool during milling is required [DAVIS 1995] [Tso 2002]. In this work, five end mills with PCD brazed inserts sharpened by different electrical technologies were designed and then produced for the experiment. Three end mills were sharpened by Electrical Discharge Machining – Grinding and the remaining two by WEDM. The comparison of these technologies of sharpening was investigated. At the end of the experiment, the temperatures in the cutting area were determined by a temperature measurement and a different geometry of the tools was also evaluated. This was based on the force loading of the tools measured by the piezoelectric dynamometer 9257B

**KEYWORDS**

PCD, electrical technologies, force loading, temperature measurement, tool geometry

## 1 INTRODUCTION

For producers of cutting tools using diamond-based materials, the requirements for sharpening and machining increase due to their specific machinability. In the past, this material was sharpened only by conventional grinding. In this technology, diamond grains bounded in the grinding wheel act on approximately equally hard PCD grains. Because of this, the grinding coefficient (G ratio) reached only 0.01 to 0.02, which was reflected mainly in the economy and machining time [DAVIS 1995]. Modern machining of these materials is based on unconventional machining methods, where the machined material – diamond – is machined in a different way than by the cutting wedge. These technologies are suitable for difficult-to-machine materials, which the diamond undoubtedly belongs to. In addition to laser technology, these include especially electrical technologies – WEDM (Wire Electrical Discharge Machining) and EDM-G (Electrical Discharge Machining). For machining process, electrical energy without conversion to mechanical energy is used. These technologies are also used for manufacturing of micro milling tools, because cutting forces acting to a tool are very slight [Gao 2013]. The diamond particles themselves are electrically non-conductive, but polycrystalline diamond contains the metallic-phase as a binder – Cobalt, which fills the interstices between diamond particles and provides the electric conductivity necessary for electrical machinability [Gao 2013] [Iwai 2013] [Tso 2002] [Yan 2013] [Yanagida 2016]. There has been much research on EDM of PCD. The following authors also dealt with this field. Gao [Gao 2013] focused on the optimal roughing and finishing process parameters of wire electrical discharge machining on PCD with grains size of 2, 10 and 25 µm. Then microtool with CTB002 – PCD material was sharpened by the optimized parameters. This tool had an edge radius 6.7 µm. Using a DoE, Fonda [Fonda 2012] also found the optimal roughing and finishing conditions for fabricating a hexagonal PCD microtool by WEDM. Tso [Tso 2002] compared conventional abrasive grinding with EDM (EDM-G) of PCD. Grinding produced a finer PCD surface than EDM-G. EDM-G resulted in a best average surface roughness **Ra** of 0.27 µm. Rahim [Rahim 2016] investigated the same comparison of the technologies based mainly on surface roughness (**Ra**), cutting forces measured through a six-channel dynamometer (Kistler 9257B), wear mode of the cutting tools, value of cutting edge radius, residual stress and level of graphitization analysed with the Raman method for three types of PCD differing in a size of grains. Yan [Yan 2013] performed an experiment to study of WEDM of PCD using a novel pulse generator. A lower value of **Ra** can be achieved as well as lower damaged layer on the machined surface of PCD. On the contrary, Iwai [Iwai 2013] improved the electric conductivity of the PCD by replacing non-conductive diamond particles with boron-doped electrically conductive diamond particles. Processing speed of this boron-doped PCD was more than seven times higher in EDM. Ullah [Ullah 2015] also focused on increasing of el. conductivity of diamond by boron doping. Yanagida [Yanagida 2016] investigated the electrical discharge machinability of PCD in different types of dielectric working fluid and the corrosion suppressing method in water. Electrochemical corrosion of cobalt can be suppressed in ultrapure water with high resistivity. Diamond materials are not a closed group of cutting materials. Besides other things, a binder is also examined in terms of mechanical and thermal properties of the whole mass of PCD. This also influences the PCD unconventional machinability. Westraadt [Westraadt 2007] study the synthesis and thermal stability of polycrystalline diamond (PCD) using CaCO3 as a sintering aid at 8 ± 0.5 GPa and 2000–2200 °C in a multi-anvil press. Akaishi et al. [Akaishi 1996] investigated the sintering behaviour of natural diamond powder with magnesium carbonate (MgCO3) as a sintered agent at the pressure of 7.7 GPa and temperature of 1800–2450 °C. Meng [Meng 2015] also study thermal stability of a diamond material – Ultrahard Polycrystalline Diamond (UHPCD), which is composed of the polycrystalline diamond (PCD) and chemical vapor deposition (CVD) diamond.

The study of diamond-based cutting material is still a topical science field. Optimal sharpening technology and tool geometry are still being explored and material area of workpiece could be also expanded, due to specific conditions during machining - cryogenic cooling [Schoop 2017] etc.

## 2 CONSTRUCTION AND SHARPENING OF TOOLS

Five end right-hand mills with different geometry sharpened by different technology – WEDM and EDM-G were the subject of the experiment. A scheme of these tools with brazed inserts can be seen in Figure 1. The end mills were designed as one-toothed due to the high wear resistance of PCD inserts. The dimension of the cutting edge diameter was increased compared to the straight shank to achieve the desired cutting speed for milling the definite workpiece. The cutter sets differ in the tool back rake ($\gamma_p$), which is little bit variable for all points of the insert. Because of this, is mentioned average value of

each tool. In this case, the tool back rake has the same value as tool cutting edge inclination, because the tool cutting edge angle ($\kappa_r$) is 90° for all end mills. One set of end mills has the angle of 0°, the second of -5° and the fifth individual end mill has the angle of 54°. Due to extreme cutting angles of the end mill *54AX*, this tool could not be sharpened by WEDM – also one toothed end mill with definite overlapping of inserts. In this particular case – this end mill could be designed only as one tooth, due to the high tool back rake, the small cutting diameter of the tool and the standard height of the insert (allowing several resharpening). The plates were cut by laser from a circular blank, which contains a flat layer of polished PCD sintered to the base of the sintered carbides. All cutters have two major flanks. The first tool side clearance $\alpha_{f1}$ on the PCD layer has a value of 10° and the second tool side clearance $\alpha_{f2}$ has a value of 14° and starts at the sintered carbide at a distance of 0.6 mm from the tool major cutting edge. The length of the tool minor cutting edge is 0.6 mm. Tool minor cutting edge angle ($\kappa_r'$) is 0°. Fanuc ROBOCUT α-600iA was used for WEDM along with an additional device for eroding rotary tools. Eroding was performed with three cuts.

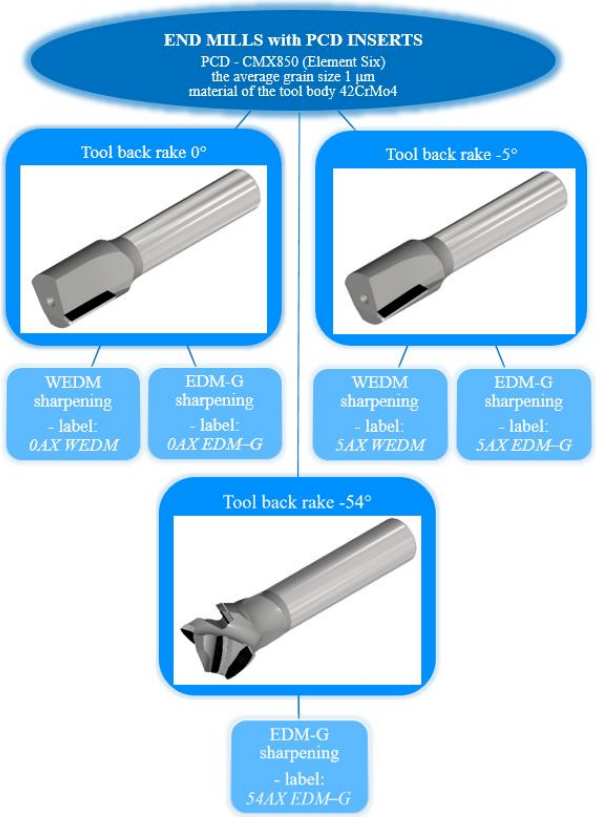


**Figure 1.** Types of Tool

In the case of EMD-G, Vollmer QXD 250 and the copper-tungsten alloy wheel electrode were used. The first major flank was also eroded by two cuts as in the case of WEDM, but the second major flank was machined by the abrasive wheel on the same machine. The end mill *54AX EDM-G* was only eroded by 2 + 1 cuts. Next machining process was the check of unbalancing, eventually its re-balancing to a degree of out-of-balance G 6.3.

## 3 ANALYSIS OF MANUFACTURED TOOLS

The cutting edge diameter of all end mills was sharpened at a tolerance of 0 to +0.04 mm (blue background in Figure 2) from a nominal dimension of the cutting tool diameter of 18 mm. The circumferential radial runout to the tool axis 0.01 mm was also fulfilled for the end mill labelled as *54AX EDM-G*. According to the result protocols from Zoller Genius 3s optical device, the inserts were measured in six positions where the runout was due to segmented inserts. The maximum inaccuracy of the cutting edge diameter was 0.004 mm for all points of the undivided single insert of the rest of the 4 mills. This data can be seen in Figure 2. The nominal values of the tool angle of the end mills in each set were the same. Small deviations were caused due to production inaccuracy.

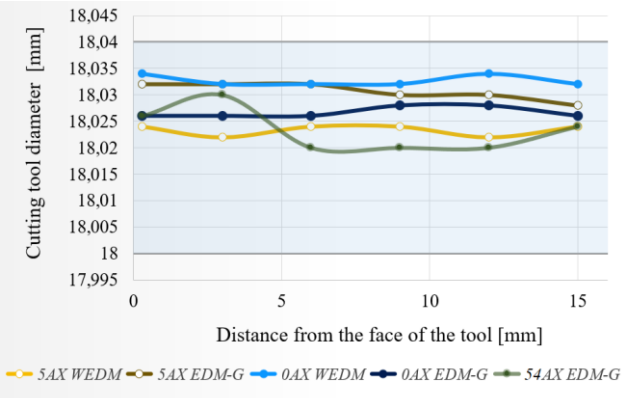


**Figure 2.** Measured Values of Cutting Tool Diameter

The tool clearances of all cutters was designed the same. The sets only differ in the angles of the rake. The mills with the tool back rake of 0° have a constant tool side rake $\gamma_f$ with a value of 10°, whereas the angle $\gamma_f$ of the non-zero tool back rake differs at each given point of the major cutting edge. As in the case of end mill with a zero $\gamma_p$, the value at the tip of the inserts is 10°, however the increasing value of $a_p$ decreases this angle due to the negative $\gamma_p$. This makes the cutter more negative both in radial and axial direction. However, the positive angle $\gamma_f$ is ensured for all points of the cutting edge, which is required for the given workpiece material – PVC [AK Plast s.r.o. 2017]. This is schematically plotted in Figures 11. Even though the situation is similar, the tool side rake of the mills *54AX EDM-G* is more variable, which will be explained later. This data was also obtained from the measurement protocols measured on the ZOLLER Genius 3s optical and measuring and inspection machine. Measured data is graphically plotted in Figure 3 and Figure 4.

Some of these facts were mentioned in the previous study [Trcka 2018] but is necessary to mention them again for the experiment as stated in this article.

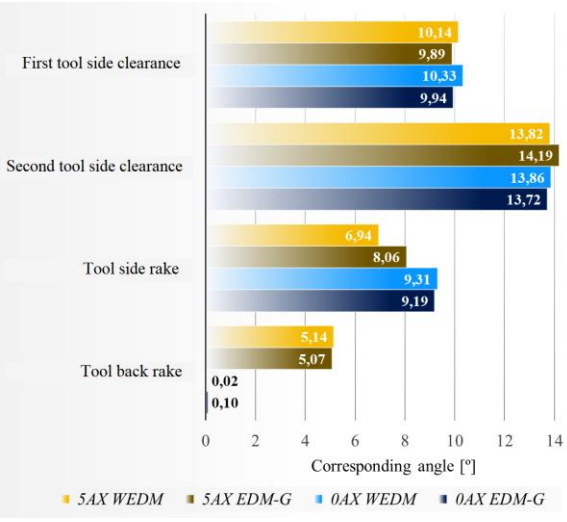


**Figure 3.** Summary Graph of Tool Angles sets *0AX* and *5AX*

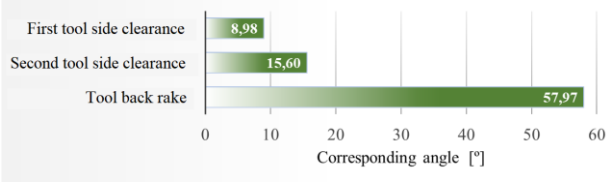


**Figure 4.** Graph of Tool Angles for end mill *54AX EDM-G*

The topography images of the first major flanks sharpened by both electrical technologies are shown in Figure 5 and Figure 6. Further analysis of these surfaces by contacting and optical methods was investigated [Trcka 2018]. Values of the rounded cutting edge radius were obtained from a non-contact optical microscope Alicona Infinite Focus 5 - IF-Edge Master Module. These can be seen in Table 1.

| | 0AX EDM-G | 5AX EDM-G | 0AX WEDM | 5AX WEDM |
|---|---|---|---|---|
| Rounded cutting edge radius [μm] | 2,48 | 2,49 | 3,15 | 3,50 |

**Table 1.** The Rounded Cutting Edge Radius of Each Tool

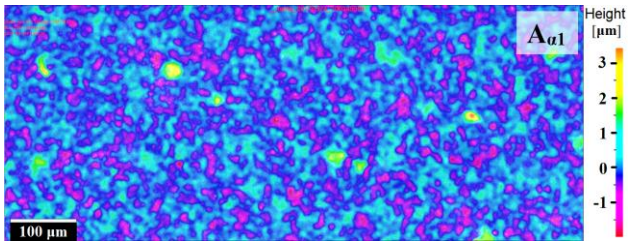


**Figure 5.** The Surface of The First Major Flank Sharpened by EDM-G Technology

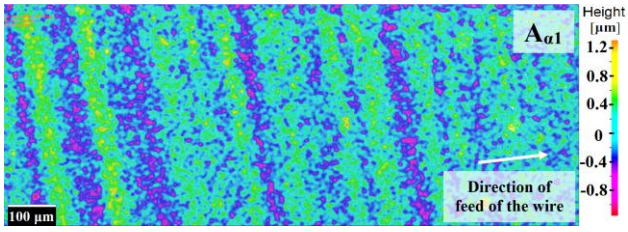


**Figure 6.** The Surface of The First Major Flank Sharpened by WEDM Technology

## 4 CUTTING CONDITIONS

The material of the workpiece used throughout the experiment was extruded thermoplastic –PVC. This material was selected based on the cutting material and available resources. Its format was a board with a thickness of 20 mm. The cutting conditions are shown in the following Table 2. These parameters are generally recommended for machining PVC. The revolutions of the spindle were recalculated based on the recommended cutting speed [AK Plast s.r.o. 2017] and operating conditions of the machine. These cutting conditions were checked for the achieved surface roughness of the machined surface by a full factorial design in the previous article [Trcka 2018] where 4 factors were selected at two levels. Axial depth of cut was chosen 3 mm, because end mill labelled as *54AX EDM-G* cuts only by one tooth up to 3,5 mm of $\mathbf{a_p}$. As it has been mentioned, there is a definite overlapping of the inserts.

| | Quantity | Unit | Value |
|---|---|---|---|
| Revolutions of the spindle | n | [$min^{-1}$] | 15 000 |
| *Cutting speed* | $v_c$ | *[$m \cdot min^{-1}$]* | *848* |
| Feed per tooth | $f_z$ | [mm] | 0,3 |
| *Feed rate* | $v_f$ | *[$mm \cdot min^{-1}$]* | *4 500* |
| Axial depth of the cut | $a_p$ | [mm] | 3 |
| Radial depth of the cut | $a_e$ | [mm] | 4 |
| Cutting fluid | | Dry | |
| Air cooling with atmospheric pressure | | | |
| Climb milling | | | |

**Table 2.** Cutting Parameters

## 5 FORCE LOADING

The following analysis consisted of an evaluation of a different geometry of *EMD-G* end mills since the *54AX* cutter was only sharpened by this electrical technology. An analysis of the force loading during 112 minutes of machining by the end mills sharpened by different electrical technologies was provided in the previous study [Trcka 2018].

All measurements were conducted on the 5-axis CNC milling machine Tajmac-ZPS MCV 1210 with the SINUMERIK control unit by piezoelectric dynamometer Kistler type 9257B. The schematic and realistic settings for force recording can be seen in Figures 7 and 8. Cutting and measuring conditions were the same for all milling cutters. No signs of vibration were seen for any end mill - during the machining and after the machining (machined surfaces, cutting edge chipping etc.). The sampling frequency was calculated with respect to the milling conditions and the required number of measurement points while the tool was in engagement.

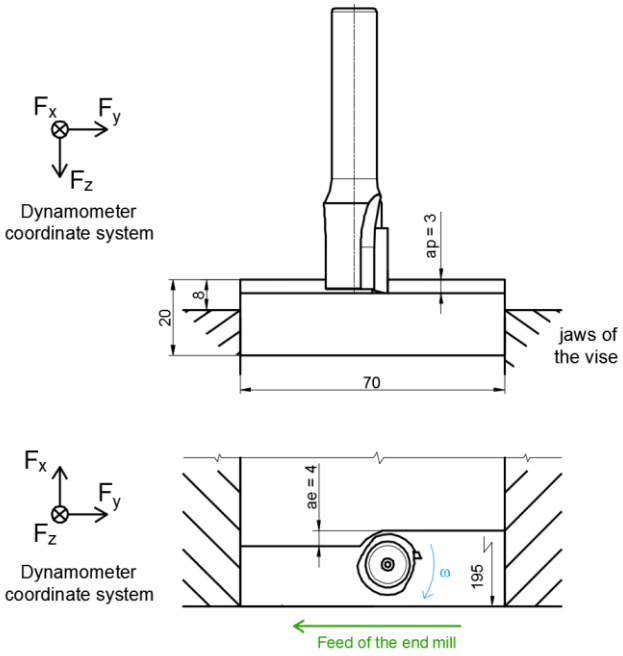


**Figure 7.** Milling Scheme for Force Recording

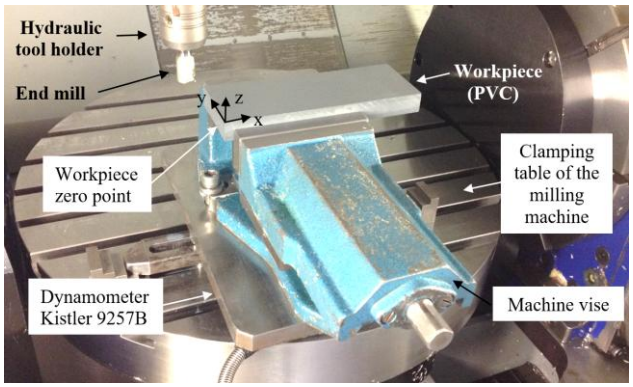


**Figure 8.** Setting for Force Load Measurement

The forces $\mathbf{F_p}$ acting in the **z**-axis direction and the forces resultant $\mathbf{F_{xy}}$ were evaluated. The force resultant in the radial plane **xy** - $\mathbf{F_{xy}}$ - is calculated from a relation (1).

$$F_{xy} = \sqrt{F_x^2 + F_y^2} \tag{1}$$

Milling forces are not constant. Their values depend on passive deformation work in chip formation, thickness of chip etc. Therefore, only one maximum force during one revolution of end mill was taken in account and evaluated in particular directions. Figure 9 shows a boxplot of the passive forces of the individual milling cutters. The positive value is oriented toward the workpiece. The increasing negative tool back rake of the milling cutters indicates a higher *positive* value of force. The dynamometer coordinate system is indicated in Figure 7. Forces act on the tool in order to insert the tool into the clamp. On the contrary, forces act on the workpiece pushing it into the bottom stop on the machine vice. Thus, the force $\mathbf{F_p}$ affects the negative tool back rake of the insert due to increased friction and forming of chips.

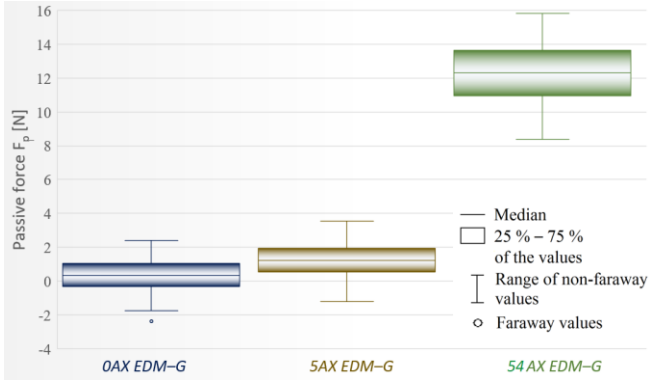


**Figure 9.** Boxplot of Passive Forces of Individual Milling Cutters

The left part of Figure 10 shows the value of the individual $\mathbf{F_{xy}}$ forces. Since the values are quite unclear, the unfiltered data of the **x** and **y** axes was taken into account. The force values of **y** axis were comparable for all cutters. The $\mathbf{F_x}$ forces were different and therefore the forces that can be seen in the right part of the picture were also evaluated. They have a similar trend as the $\mathbf{F_{xy}}$ forces. That signifies that the force of $\mathbf{F_y}$ of individual mills does not really differ fundamentally. Different **x**-axis forces are caused by the tool side rake. As it has been mentioned in Chapter 3, *0AX* cutters have this angle of 10° and is constant. Regarding the *5AX* cutter, this angle decreases with an increasing $\mathbf{a_p}$ value at a given point of cutting edge. The $\mathbf{\gamma_f}$ of 10° is achieved at the tip of the tool, while at $\mathbf{a_p}$ 3 mm this value is 8.5° according to the 3D model. The $\mathbf{\gamma_f}$ of the cutter *54AX* also decreases with an increasing $\mathbf{a_p}$ size.

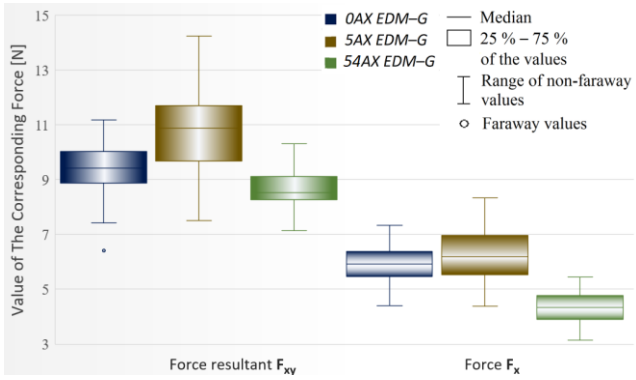


**Figure 10.** Boxplot of Forces In The Radial Plane of Each Cutter

This tool with a high $\mathbf{\gamma_p}$ must have a high tool side rake at the tip to obtain a positive angle of all range of engagement within one insert. Specifically, the $\mathbf{\gamma_f}$ is 43° at the tip of the tool, while at an axial distance of 3 mm from the tip, this angle is just 13.5° according to the 3D model. The mean values of the tool side rake of the individual cutters at point **O** are schematically plotted in Figure 11. For clear arrangement, the applied forces are drawn at the **O´** point and the effect of the rounding of the cutting edge, friction, etc. are neglected. As it can be seen, the increasing angle $\mathbf{\gamma_f}$ decreases the force component of the **x**-axis. Positive geometry in the side (radial) plane generally contributes to the decrease in $\mathbf{F_{xy}}$ forces, as shown in Figure 10.

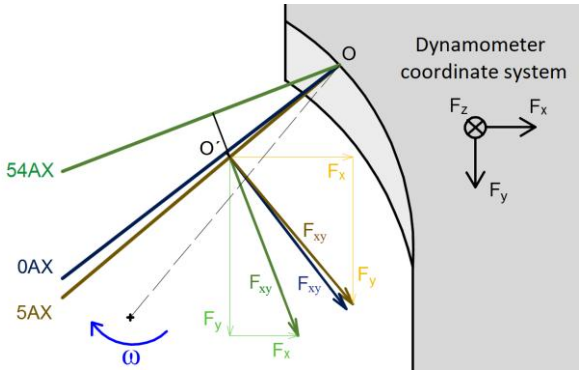


**Figure 11.** Influence of The Angle $\mathbf{\gamma_f}$ On The Ratio of The Sizes of The Individual Force Components.

The surface machined by the cutter of sets *0°* and *5°* showed a bright, comparable appearance. However, the surface machined by the *54AX EDM-G* cutter showed a very matt appearance - Figure 12. This is due to the high tool back rake that causes forming of chips. During the cutting of this face surface there is no real cutting action, but rather *forging* - forming the surface. For these reasons, this tool for shoulder milling uses a separate insert with positive geometry. The combination of positive tool back rake on the tool minor cutting edge and the negative tool back rake on the tool major cutting edge ensures no burrs at the top surface of workpiece and at the same time the machined surfaces has a high quality of surface.


**Figure 12.** Face Surface Machined by Mill *54AX EDM-G*

It is clear from the evaluated records that the total cutting force **F** of the 54AX EDM-G cutter is the highest and the smallest with the tool back rake of 0°. The total cutting force is force resultant of all 3 individual forces and is calculated from a relation (2).

$$F = \sqrt{F_x^2 + F_y^2 + F_p^2} \qquad (2)$$

The dominant component of the total cutting force is the component $\mathbf{F_p}$. With a more negative geometry, a higher force is required to remove the same workpiece material under the same milling conditions, thereby also increasing the required power of the electric motor. This is the result of a more problematic chip formation and *forging*.

## 6 THERMAL IMAGING

Experimental temperature measurement was performed using the thermal imaging camera ImageIR 8300 hp of the company Infratec. The camera captures the temperature on the principle of infrared radiation. It is that part of the electro-magnetic spectrum that connects on the visible spectrum to the red light at a long wavelengths (760 nm) and continues up to a wavelength of approx. 1 mm. Camera recording parameters were set according to cutting conditions to meet the quality of recorded records. The image saving frequency was increased due to the high number of spindle revolutions. That resulted in a higher number of images during one revolution of the cutter. This was finally set at 1.2 kHz and the sequencing time had a value of 94 µs. The resolution size was set according to the cutting conditions and the length of the milled workpiece to 640 x 116. The experiment was carried out under the same cutting conditions as the force measurement, with the difference that the machine vice was rotated on the milling table of 90° due to visibility of the cutting area for the thermal imaging camera – Figure 13. The software Irbis 3.1 InfraTec professional was used for capturing and evaluating records. End mills sharpened by the *EDM-G* were subjected to this measurement. The aim of the evaluation was to determine the maximum temperatures of chips separated by the cutting edge of the individual end mills and to find continuity with the already measured force loading. The emissivity for the workpiece material was set to PVC 0.92, as this value is stated to be between 0.91-0.93 [ThermoWorks 2018]. The evaluated records in Figure 14 show that the increasing tool back rake causes the rising of the chip temperature. This is the result of forming of chips, which causes higher friction, deformation work and hence also increase of the temperature in the cutting area. The difference in the maximum temperature between the cutter with the tool back rake 0° and 54° is 21 °C. Therefore, the temperature corresponds to the force loading of the end mills. The chips temperature of all cutters is greater than the softening temperature of PVC according to Vicat. This may be

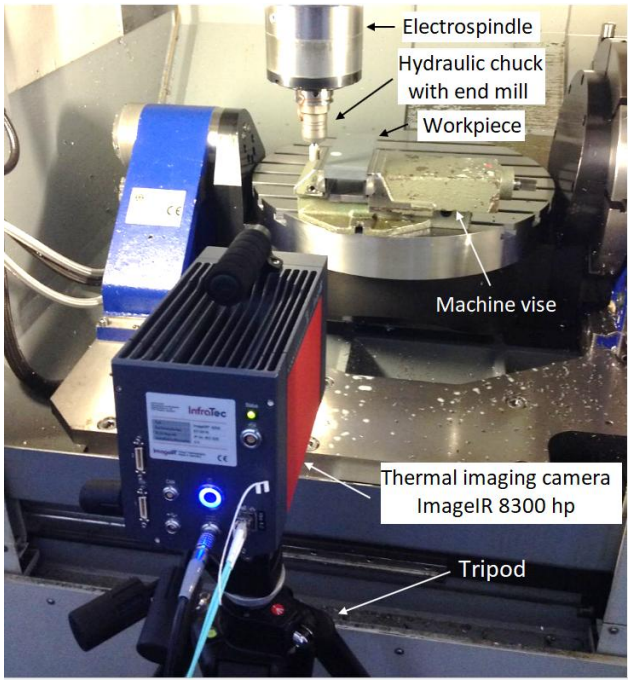


**Figure 13.** Setting for The Temperature Measurement

the reason why the cutting forces dropped in the middle of the experiment in prevous study [Trcka 2018], but this can not be said unambiguously due to the temperature measurement only conducted at the end of the experiment and not at the beginning of the 112 minute experiment.

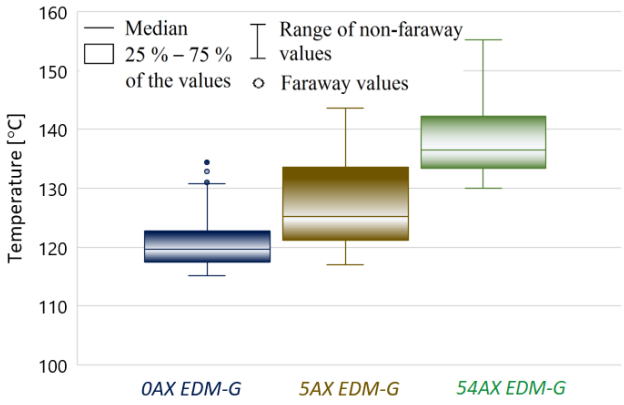


**Figure 14.** Maximum Temperatures of End Mills sharpened by EDM-G

While measuring the temperature, the effect of the value of spindle revolutions of an electric motor on the chip temperature was also measured. This was done for one cutter, namely *0AX EDM-G.* Figure 15 shows that the spindle revolutions of 18 000 $min^{-1}$ reduced the chip temperature. This is due to the shorter contact of the milling cutter with the workpiece. The value of spindle revolutions were chosen to be higher than the experimental value of 15 000 $min^{-1}$, because the PCD cutting inserts allow higher cutting speeds for PVC milling. Spindle revolutions of 18 000 $min^{-1}$ correspond to a cutting speed of 1017 $m \cdot min^{-1}$.

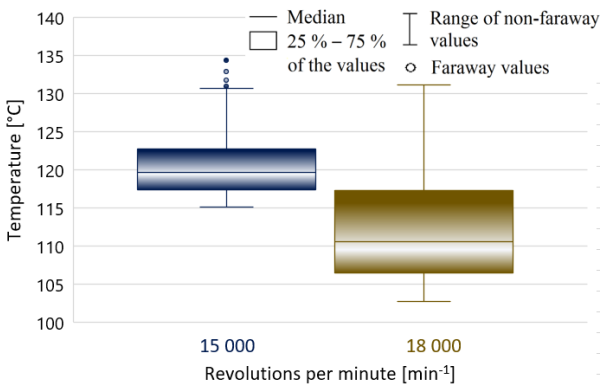


**Figure 15.** Influence of The Value of Revolutions on The Temperature of Chips

From the obtained records, it could be observed that the highest workpiece temperature was in the corner of the milled shoulder - i.e. the intersection of the face and peripheral surfaces. This is due to the fact that PVC has a low thermal conductivity **λ**, which makes the heat not to go into the workpiece but into the environment. The slowest airflow occurs in the corner. Figure 16 shows a temperature field with a color scale in which the three measured locations defined by the line segments **L1**, **L2** and **L3** were selected. Figure 17 complements in detail the information of the previous Figure with the location and value of the maximum temperatures in each segment - the corner of the shoulder. The temperature distribution in the individual sections is graphically plotted in Figure 18.

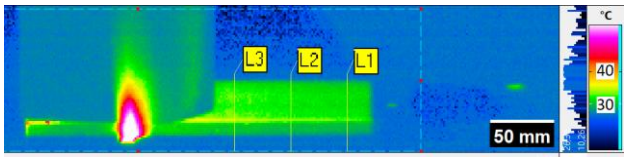


**Figure 16.** The Temperature Field of The Cutter While Machining

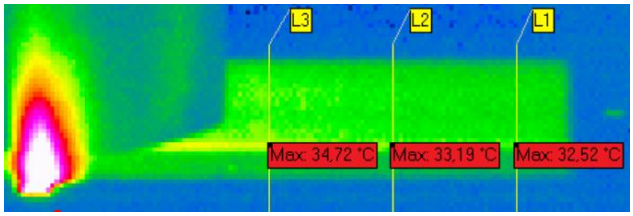


**Figure 17.** Maximum Temperature Locations on Selected Line Segments

The highest temperatures are also reached immediately after material separation in this location. As a result, the tip of the insert is the most heat and pressure loaded. In addition, the negative tool back rake causes the material to move to the face of the cutter. Images of major flanks of the tools were taken from the optical measurement by the microscope at the beginning and after 112 minutes of machining - Figures 19 and 20. As it can be seen, the tip of the insert is the most worn out. All end mills of the tool life experiment had the same trend of wear.

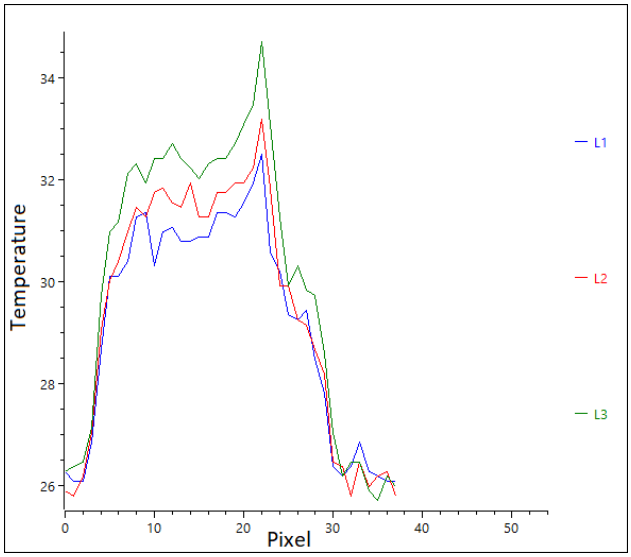


**Figure 18.** Profile Chart of The Temperatures of Individual Section

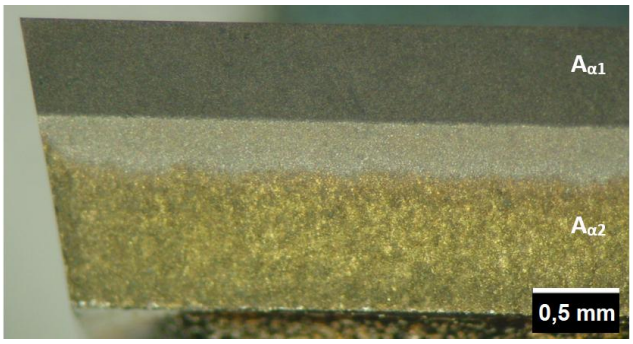


**Figure 19.** Flank Faces of New Sharpened Tool Labelled as *0AX WEDM*

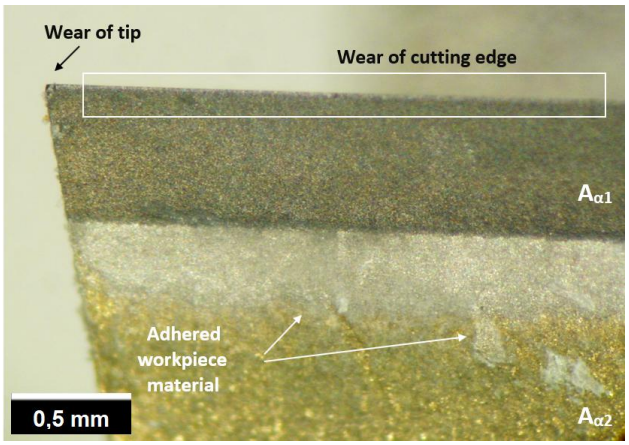


**Figure 20.** Flank Faces of End Mill *0AX WEDM* After 112 Minutes of Machining

## 7 CONCLUSION AND DISCUSSION

• All end mills were optically measured - the dimension of the cutting edge diameter and the tool angles, which we needed to verify for further analysis.

• Under given sharpening conditions, the values of the rounded cutting edge radius of the end mills sharpened by EDM-G were 2,48 µm and 2,49 µm and for the WEDM process 3,15 µm and 3,50 µm.

• Topography of eroded first major flanks in the WEDM method had a wavy structure caused by the feed and tension of the wire, while in the case of the second method, it was possible to see a regular appearance of craters after torn grains.

• The chip temperature measurement during machining showed that the more negative geometry in the back direction means higher temperatures. In this case, the temperature corresponds to the force loading of the individual milling cutters because the end mill with more negative geometry in the back direction also achieves higher total cutting force during machining. This is the result of forming of chips, which causes higher friction and also deformation work.

• More positive geometry in the tool side plane meant reducing cutting forces in this direction.

• The increasing value of spindle revolutions reduced the chip temperature leaving the tool as the tool was in contact with the workpiece for a shorter time.

• The highest workpiece temperature was measured at the corner of the milled shoulder, where the greatest load on the cutting edge is also generally occurring. Images from the optical microscope confirmed a wear on the tip of the tool. Due to the long tool life of PCD inserts, the wear on the flanks was minimal and almost invisible by a conventional light microscope.


## ACKNOWLEDGMENTS

This article was supported and co-financed from a specific research FSI-S-16-3717 called "Research in Field of Modern Production Technologies for Specific Applications".
The results of this project NETME CENTRE PLUS (LO1202) were obtained with the financial support of the Ministry of Education, Youth and Sports under the targeted support of the "National programme of sustainability I."
The milling tools were produced by Vydona s.r.o. headquartered in Pravčice near Kroměříž. The company also funded the milling process and performed a control measurement on the Zoller Genius 3s optical device.


## REFERENCES


[Akaishi 1996] Akaishi, M. and Yamaoka, S. Physical and chemical properties of the heat resistant diamond compacts from diamond-magnesium carbonate system. Materials Science and Engineering: A, May 1996, Vol.209, No.1-2, pp 54-59. ISSN 0921-5093

[AK Plast s.r.o. 2017] AK Plast s.r.o. Directive on machining (in Czech). AK Plast s.r.o., 2017, Ledec nad Sazavou [online]. © 1995 - 2017 [5. 7. 2017]. Available from <http://www.akplast.cz/smernice-pro-obrabeni>
<https://www.thermoworks.com/emissivity_table>

[Davis 1995] Davis, J. R. Tool Materials. ASM Specialty Handbook. Ohio: ASM International, 1995. ISBN 0-87170 545-1

[Fonda 2012] Fonda, P., Katahira, K., Kobayashi, Y. and Yamazaki, K. WEDM condition parameter optimization for PCD microtool geometry fabrication process and quality improvement. The International Journal of Advanced Manufacturing Technology, 2012, Vol.63, No.9-12, pp 1011 1019

[Gao 2013] Gao, C., Zhan, Z., Wang, S., He, N. and Li, L. Research on WEDM Process Optimization for PCD Micro Milling Tool. Procedia CIRP, 2013, Vol.6, pp 209-214. ISSN 2212-8271

[Iwai 2013] Iwai, M., Ninomiya, S. and Suzuki, K. EDM Properties of Newly Developed PCD Made Up of Electrically Conductive Diamond Particles. Procedia CIRP, 2013, Vol.6, pp 140-145. ISSN 2212-8271

[Meng 2015] Meng, D., Yue, W., Lin, F., Wang, C. and Wu, Z. Thermal stability of ultrahard polycrystalline diamond composite materials. Journal of Superhard Materials, March 2015, Vol.37, No.2, pp 67-72. ISSN 1934-9408

[Miller 2010] Miller, I. DOE: Design and analysis of experiments with MINITAB© (in Czech). Praha: Interquality, spol. s.r.o., 2010. ISBN 987-80-902770-5-2

[Rahim 2016] Rahim, M. Z., Li, G., Ding, S., Mo, J. and Brandt,M. Electrical discharge grinding versus abrasive grinding in polycrystalline diamond machining—tool quality and performance analysis. The International Journal of Advanced Manufacturing Technology, July 2016, Vol.85, No.1-4, pp 263 277

[Schoop 2017] Schoop, J., Sales, W. F. and Jawahir, I. S. High speed cryogenic finish machining of Ti-6Al4V with polycrystalline diamond tools. Journal of Materials Processing Technology, December 2017, Vol. 250, pp 1-8. ISSN 0924-0136

[ThermoWorks 2018] ThermoWorks. Emissivity Table. ThermoWorks, 2018, Utah, USA [online]. © 2018 [3. 1. 2018]. Available from <https://www.thermoworks.com/emissivity_table>

[Trcka 2018] Trcka, T., Polzer, A. and Sedlak, J. End mills with PCD inserts sharpened by different electrical technologies. MM Science Journal, March 2018. DOI:10.17973/MMSJ.2018_03_201759, ISSN 1805-0476

[Tso 2002] Tso, P.-L. and Liu, Y.-G. Study on PCD machining. International Journal of Machine Tools & Manufacture, February 2002, Vol.42, No.3, pp 331-334. ISSN 0890-6955

[Ullah 2015] Ullah, M., Ahmed, E., Hussain, F., Rana, A.M. and Raza, R. Electrical conductivity enhancement by boron-doping in diamond using first principle calculations. Applied Surface Science, April 2015, Vol.334, pp 40-44. ISSN 0169-4332

[Westraadt 2007] Westraadt, J. E., Dubrovinskaia, N.,Neethling, J. H. and Sigalas, I. Thermally stable polycrystalline diamond sintered with calcium carbonate. Diamond and Related Materials, November 2007, Vol.16, No.11, pp 1929–1935. ISSN 0925-9635

[Yan 2013] Yan, M.-T., Fang, G.-R. and Liu, Y.-T. An experimental study on micro wire-EDM of polycrystalline diamond using a novel pulse generator. The International Journal of Advanced Manufacturing Technology, June 2013, Vol.66, No.9-12, pp 1633-1640

[Yanagida 2016] Yanagida, D., Minami, H. and Watanabe, K. Electrical Discharge Machining of PCD in Ultrapure Water. Procedia CIRP, 2016, Vol.42, pp 292-296. ISSN 2212-8271


## CONTACT:


Ing. Tomas Trcka
Brno University of Technology
Faculty of Mechanical Engineering
Technicka 2896/2, 616 69 Brno, Czech Republic
e-mail: 153306@vutbr.cz